Nanoscale

PAPER

View Article Online
View Journal | View Issue

Cite this: *Nanoscale*, 2023, **15**, 6170

Selective recognition of the amyloid marker single thioflavin T using DNA origami-based gold nanobipyramid nanoantennas†

Charanleen Kaur, Vishaldeep Kaur, Shikha Rai, Mridu Sharma and Tapasi Sen *

The development of effective methods for the detection of protein misfolding is highly beneficial for early stage medical diagnosis and the prevention of many neurodegenerative diseases. Self-assembled plasmonic nanoantennas with precisely tunable nanogaps show extraordinary electromagnetic enhancement, generating extreme signal amplification imperative for the design of ultrasensitive biosensors for point of care applications. Herein, we report the custom arrangement of Au nanobipyramid (Au NBP) monomer and dimer nanoantennas engineered precisely based on the DNA origami technique. Furthermore, we demonstrate the SERS based detection of thioflavin T (ThT), a well-established marker for the detection of amyloid fibril formation, where G-Quadruplexes govern the site-specific attachment of ThT in the plasmonic hotspot. This is the first study for the SERS based detection of the ThT dye attached specifically using a G-Quadruplex complex. The spectroscopic signals of ThT were greatly enhanced due to the designed nanoantennas demonstrating their potential as superior SERS substrates. This study paves the way for boosting the design of next-generation diagnostic tools for the specific and precise detection of various target disease biomarkers using molecular probes.

Received 15th November 2022,
Accepted 25th February 2023

DOI: 10.1039/d2nr06389a

rsc.li/nanoscale

1 Introduction

Alzheimer's disease, Parkinson's disease, and type II diabetes are just a few of the incurable diseases caused by protein misfolding that have become significant health issues.[1] Since the early diagnosis of such neurodegenerative diseases is crucial, substantial research is being conducted to improve the existing approaches for early detection and finding new potential biomarkers of the diseases.[2] Therefore, finding reproducible and trustworthy biomarkers that can improve the diagnosis of such diseases is crucial for beginning the treatment at the earliest feasible stage and monitoring the therapeutic efficacy. Being the first step in the diagnosis, the very sensitive identification of neurological illness biomarkers is crucial. In various neurodegenerative disorders, normally soluble proteins undergo aggregation and are converted into amyloid fibrils.[3,4] These self-assembled β forms cause severe deteriorating effects on human health.[5] The examination of the major disorders indicated above depends on the detection, identification, and physicochemical characterisation of amyloid fibrils. The most used dye for both *in vitro* and *in vivo* detection of amyloid fibril development is thioflavin T (ThT).[6] ThT is a member of a class of molecules called molecular rotors,[7] which can also function as viscosity sensors. ThT exhibits enhanced fluorescence and suppression of twisted internal charge transfer (TICT) when it is exposed to amyloid fibrils or highly viscous liquids. This is the main basis for using this dye to find amyloid fibrils. If the dye is incorporated into the beta-sheet-rich structures of amyloid fibrils, it significantly increases their fluorescence. ThT is commonly used to detect the presence of senile plaques in Alzheimer's disease (AD). The angle between benzothiazole and dimethylaniline rings changes after the interaction.[8,9] ThT has been extensively used for the detection of amyloid fibrils.[10–12] ThT detection has also been well established with a G-quadruplex using fluorescence as a characterization tool.[13,14]

For the early detection of clinically important biomarkers, there is a need for using highly sensitive measurement techniques. Surface-enhanced Raman spectroscopy (SERS) is a sensitive optical technique that enables the ultrasensitive detection of molecules even at the single molecule level.[15,16] It is based on the concepts of chemical enhancement and electromagnetic field amplification near metallic structures. In several studies, SERS has been successfully used for the highly sensitive detection of various biomolecules of interest, demonstrating enormous potential in biomedical research.[17–19] This vibrational spectroscopy involves the use of localized surface

Institute of Nano Science and Technology, Sector-81, Mohali, Punjab – 140306, India. E-mail: tapasi@inst.ac.in

† Electronic supplementary information (ESI) available. See DOI: https://doi.org/10.1039/d2nr06389a

plasmons of metal nanostructures for generating sensitive fingerprints of analytes. Anisotropic gold (Au) nanostructures possess higher electromagnetic field enhancement than spherical nanoparticles due to the presence of hotspots and the hotspot strength depends on the geometry of the metal nanostructures.[20,21] Spherical silver (Ag) nanoparticles were used for vibrational characterization of ThT using SERS and the lowest detectable concentration of ThT was found to be 10^{-9} M.[6] Maiti *et al.* further carried out concentration dependent SERS measurement of ThT using Au and Ag nanoparticles indicating a picomolar detection limit.[22] Altuntas *et al.* developed multibranched nanopillared surfaces and demonstrated the ultrasensitive detection of amyloid fibrils of up to 0.5 pg ml^{-1} using thioflavin T as a marker.[23] Hollow Au Ag nanostars were used for ThT detection up to a minimum concentration of 10^{-8} M.[24] SERS-based single molecule detection has also been reported in the literature using assembled plasmonic nanoantennas having tunable nanogaps majorly formed using Au and Ag anisotropic nanostructures.[25,26] Precise placement of biomolecules at the plasmonic hot-spot volume that yields the greatest field enhancement is a prerequisite for this SERS-based approach to achieve the maximum Raman scattering signal required for single-molecule sensitivity detection. DNA origami-based plasmonic nanostructures have stood out among various SERS-active nanostructures by demonstrating their use in the single-molecule detection of dyes, proteins, and other important compounds. This arises from the precise addressability offered by DNA clamps in DNA origami design, enabling nanoscale precision for the positioning of biomolecules of interest specifically at the hotspots of the assembled plasmonic nanostructures.[27–30] Previously, our group reported the assembly of Au (core)- Ag (shell) nanostars on DNA origami for the ultrasensitive detection of a bacterial biomarker, pyocyanin.[31] Recently we used these nano-assemblies for the detection of the catecholamine neurotransmitter dopamine.[32] Furthermore, SERS based enhancement of a single biologically relevant thrombin protein positioned using aptamers at the junction of the assembled bimetallic nanostars on DNA origami was demonstrated.[33]

Recently, gold nanobipyramids (Au NBPs) have stood out among other anisotropic structures by exhibiting even greater local field enhancement, larger optical cross sections, narrower resonances, excellent shape uniformity, and higher sensitivity to refractive index changes compared to nanorods. They therefore appear to be excellent candidates for a variety of biophotonic and spectroscopic applications.[34–36] In a recent report, Au NBPs have been found to show a 10-fold higher enhancement factor as compared to nanorods.[37] Amin *et al.* used these structures for detecting drug additives such as thiram and bisphenol-S.[38] Very recently, Dong *et al.* assembled Au NBPs into chiral plasmonic nanostructures using DNA origami demonstrating their superior chiroptical response.[39] These new structures have been used for achieving a high photothermal response[40] and refractive index sensitivity[41] and have been used as outstanding SERS substrates.[42,43]

In this study, we demonstrate for the first time the design of gold bipyramid monomer and dimer structures with precise nanogaps assembled on a rectangular DNA origami template. An amyloid marker, ThT, a SERS-active dye, was incorporated into DNA origami using a G-rich DNA sequence modified branching staple in the junction of the origami. The stoichiometry of the ThT dye molecule bound to the G-quadruplex complex was estimated using a single molecule confocal fluorescence microscope which suggested the presence of single ThT molecules incorporated into DNA origami. We further used our designed nanoantennas for the specific detection of ThT by the SERS based technique for achieving the goal of ultrasensitive detection of amyloid fibrils. Our experimental findings prove that our developed platform was able to sense single ThT molecules through extraordinary enhancement of the ThT Raman signal by the plasmonic hotspot created in the nanogap of Au NBP dimer nanoantennas. To the best of our knowledge, this is the first report on the specific detection of single ThT using metallic nanoantennas based on DNA origami. Our present work therefore suggests that the as-developed DNA origami based nanoantennas can serve as a platform for the specific detection of important biomarkers of diseases at the single molecule level and can also be extended to study the interaction of biologically important molecules with external stimuli at the single molecule level.

2 Materials and methods

2.1 Materials

Gold(III) chloride trihydrate ($HAuCl_4 \cdot 3H_2O$, ≥99.9%), silver nitrate ($AgNO_3$), cetyltrimethylammonium chloride solution (CTAC, 25 wt%), trisodium citrate dihydrate, ascorbic acid, sodium borohydride ($NaBH_4$), biotin labeled albumin, sodium dodecyl sulphate (SDS), tris(hydroxymethyl)aminomethane (Tris base), disodium ethylenediaminetetraacetic acid (EDTA), phosphate buffer saline (PBS), tris(carboxyethyl)phosphine hydrochloride (TCEP·HCl), sodium chloride (NaCl), magnesium chloride hexahydrate ($MgCl_2 \cdot 6H_2O$) and thioflavin T (ThT) were obtained from Sigma-Aldrich. Cetyltrimethylammonium bromide (CTAB, 99%) was purchased from SRL. Hydrochloric acid (HCl, 37%), hydrogen peroxide (H_2O_2, 30%), ammonia solution (25%), ethanol, and potassium chloride KCl (99–100%) were procured from Merck. NeutrAvidin protein and Lab-Tek chambered coverglass were purchased from Thermo Fisher Scientific. The M13mp18 Single-stranded DNA was procured from New England Biolabs (NEB) and used without purification. The staple strands, modified staples and aptamer sequence were procured from Integrated DNA Technologies (IDT) and used without further purification. HPLC purified thiolated DNA oligonucleotides and modified staple strands were obtained from Metabion (Germany). Sephacryl S-300 high resolution resin was purchased from GE Healthcare. Carbon coated Cu TEM grids were purchased from Ted Pella and Si wafer was procured from Ekta Marketing Corporation. All the experiments were done using

ultrapure Milli-Q water (resistivity 18.2 MΩ cm^{-1}). All glassware used for the experiment was washed with aqua regia and dried appropriately before use.

2.2 Methods

2.2.1 Synthesis of rectangular DNA origami. The rectangular DNA origami monomer and dimer were prepared according to our previously published report.[25] Briefly, the m13mp18 scaffold was mixed with an excess of short staple strands in 1 × TAE buffer containing 12.5 mM $MgCl_2$ and subjected to annealing followed by slow cooling in a PCR thermocycler. For dimerization, DNA origami monomers were mixed with an excess of branching staples in 50 × TAE buffer containing 12.5 mM $MgCl_2$ and incubated for 24 hours. The prepared DNA origami dimer was then purified using Sephacryl S-300 resin filtration to remove excess staples.

2.2.2 Synthesis of Au nanobipyramids (Au NBPs). Monodisperse Au NBPs were synthesized using seed mediated growth according to a previously reported protocol.[44] The procedure for the twin formation of seeds was adopted from the study by Sánchez-Iglesias *et al.*[45] Briefly, an aqueous solution containing $HAuCl_4$ (50 mM, 49.6 μl), CTAC (25 wt%, 661 μl) and trisodium citrate (4.87 mM) was prepared. To this solution, ice cold $NaBH_4$ (25 mM, 250 μl) was injected quickly under stirring resulting in the formation of brownish seeds. The as synthesized light-brown seeds were then subjected to thermal treatment at 80 °C, resulting in a gradual color change from light brown to red over the course of 2 hours. After thermal treatment, Au nanoseeds were added into a growth solution consisting of CTAB (5 ml, 0.1 M), $HAuCl_4$ (250 μl, 0.01 M), HCl (100 μl, 1M), $AgNO_3$ (50 μl, 0.01M), and ascorbic acid (40 μl, 0.01M). The solution was kept at 30 °C for 2 hours. Furthermore Au NBP solution was purified by Ag overgrowth of synthesized NPs by heating at 65 °C for 3 hours in the presence of CTAC (38.4 mM). $AgNO_3$ (3.64 mM) and ascorbic acid (17.3 mM) was then added to this solution resulting in the growth of Ag on Au NBPs.[46] This was followed by centrifugation of the synthesized NBPs where spherical impurities remained in the supernatant and Au NBPs settled at the bottom. Finally, Ag was etched using a mixture of H_2O_2 (30%, 28 μl) and NH_4OH (25%, 40 μl) resulting in the formation of purified Au NBPs.

2.2.3 Synthesis of DNA functionalized Au NBPs. To prepare DNA functionalized Au NBPs, firstly deprotection was done by adding TCEP to disulfide protected thiolated DNA for 3 hours. Two different sequences of thiol DNA 5′-SH-CGTCGTAT-TCGATAGCTTAG-3′ and 5′-SH-TTGGTGGTGGTGGTGGTGGT-3′ were used. The procedure for DNA functionalization was adapted with modifications from a previous report.[47] The deprotected thiol DNA was incubated with Au BPs (1 OD) at pH 5 in 5 × TBE buffer and SDS (0.01%) overnight under slow stirring at room temperature. To enhance the DNA loading density, slow salt additions were done until a final concentration of 400 mM NaCl was reached followed by purification. The stability of as synthesized DNA functionalized Au NBPs was checked using a salt (PBS, 500 mM NaCl) test.

2.2.4 Immobilization of Au NBPs on DNA origami. Au NBPs were immobilized on DNA origami in monomer and dimer configurations. For the dimer configuration, two different sets of capturing staples were used on both origami monomers and capturing staples on only one origami monomer were used to assemble the Au NBP monomer on dimerized DNA origami. DNA functionalized Au NBPs were mixed with DNA origami in a molar ratio of 2 : 1 and 4 : 1 for monomer and dimer configurations, respectively, in TBE buffer containing 300 mM NaCl. The mixed solution was then heated repeatedly between 20 °C and 40 °C, over a course of around 12 hours. The prepared Au NBP monomer and dimer nanoantenna were then used for characterization.

2.2.5 Detection of ThT using Au NBP assemblies on DNA origami. ThT was incorporated into DNA origami using a G-rich DNA sequence modified branching staple. During dimerization, one of the branching staples at the middle of DNA origami is replaced with a G-rich DNA sequence in the presence of Tris-KCl buffer. After purification of the origami dimer, an excess of ThT solution (40 nM) was incubated overnight at room temperature followed by purification (20 nM). The prepared sample was then mixed with Au NBPs and heated repeatedly between 20 °C and 40 °C for 12 hours and further used for Raman measurements.

2.3 Characterization

2.3.1 Instrumentation. Ultraviolet-Visible (UV-Vis) absorption spectra were recorded using a Shimadzu UV-2600 spectrophotometer. TEM imaging was done using a JEOL 2100 microscope at an accelerating voltage of 120 kV for DNA origami samples and 200 kV for Au NBPs. AFM imaging was done using a Bruker Multimode 8 scanning probe microscope with TAP 150-Al-G cantilevers (Budget sensor). Raman measurements were conducted using Witec-alpha 300 R equipped with an upright optical Zeiss microscope using 633 nm excitation with a 100× objective (NA = 0.9) at room temperature. Single molecule fluorescence measurements were performed using PicoQuant Microtime 200 (Berlin, Germany) using a 100× oil objective in an Olympus IX73 inverted microscope with a piezo scanner ((P-733.2CD). The laser excitation source was a 405 nm pulsed laser diode (LDH-D-C-405S) at 20 MHz repetition rate. The laser power was adjusted using an attenuation unit and neutral density filters and set to 80 a.u. (~1 μW). The fluorescence signal was passed through a single band dichroic filter (ZT405rdc-UF3 Chroma) followed by a band pass filter (ET425lp-Chroma) and focused on a 50 μm pinhole. The signal was then passed to a single photon avalanche photodiode (SPAD) (Excelitas). Time resolved measurements were done using MultiHarp 150 (PicoQuant) with time tagged electronics. The data were analyzed using SymPhoTime 64 software.

2.4 Sample preparation

2.4.1 TEM imaging. The samples of Au NBPs were prepared by directly drop-casting the solution on a carbon coated Cu grid. For the preparation of DNA origami samples, firstly

the grid was activated using 1 M $MgCl_2$ followed by drop-casting the sample. The negative staining of samples was done using uranyl acetate (2% w/v) solution.

2.4.2 AFM and Raman imaging. The purified sample of Au NBPs–DNA origami assemblies was diluted in 10 × TAE, 200 mM $MgCl_2$ and drop-cast on plasma cleaned Si wafer (1 × 1 cm^2 size). The sample was then incubated for 2 hours in a moist chamber followed by washing with MQ water. The final concentration of ThT after immobilization of DNA origami with Au NBPs followed by dilution for single molecule SERS measurements was calculated to be ~2.6 nM. The AFM and Raman measurements were done using the prepared sample after drying.

2.4.3 Single molecule fluorescence measurements. For single molecule fluorescence measurements, 8-well Lab-Tek chambers were activated with 10% HF solution and kept for 10 min. Furthermore it was washed 5 times with syringe filtered MQ repeating the procedure again. The activated chamber was incubated with 0.5 mg ml^{-1} biotin overnight at 4 °C followed by washing with PBS buffer. The same chamber was further incubated with NeutrAvidin 0.5 mg ml^{-1} for 1 hour and washed with PBS buffer. The sample was diluted in PBS 12.5 mM $MgCl_2$ buffer and used for single molecule confocal imaging.

3 Results and discussion

3.1 Synthesis and DNA functionalization of Au NBPs

Au NBPs were synthesized using a seed-mediated growth method in aqueous solution according to the procedure reported previously.[44] The penta-twinned Au seeds were prepared through a stepwise combination of the synthesis of small-sized Au NPs followed by thermally induced twinning.[45] The twinned Au seeds were then used for the synthesis of Au NBPs using a growth solution containing CTAB, $HAuCl_4$, HCl, $AgNO_3$, and ascorbic acid. Ag^+ ions are crucial for the formation of high-quality Au NBPs since they control the dominant sites for the defect-free deposition of Au atoms.[48] The yield of as synthesized Au NBPs was improved by purification so as to remove the coexisting impurities in the form of spherical nanoparticles. The purification was done according to a previously reported method involving a step by step procedure of Ag growth, depletion-force induced self-separation and chemical etching of Ag.[49] The first step involving the overgrowth of Ag on Au BPs realized by the reduction of $AgNO_3$ in the presence of CTAC resulted in the formation of faceted Au@Ag NPs and Au/Ag heteronanorods.[50] This was followed by centrifugation where bimetallic heteronanorods were separated from Au@Ag NPs due to the depletion interactions. Subsequently, a mixture of H_2O_2 and NH_4OH resulted in the chemical etching of Ag yielding purified Au NBPs. The color of the purified solution of Au NBPs changed from pink to brown. The UV-Vis spectrum of purified Au NBPs as depicted in Fig. 1(a) shows two distinct plasmonic peaks with a transverse localized surface plasmon band (LSPR) centered at 516 nm and a longitudinal LSPR band centered at 703 nm. The representative TEM images as depicted in Fig. 1(b) and (c) confirmed the formation of Au NBPs with a high degree of monodispersity. The average size of synthesized Au NBPs as calculated from different TEM images was 75 ± 5 nm.

The synthesized Au nanobipyramids were further characterized using High-resolution TEM (HRTEM) imaging, Energy dispersive X-ray (EDX), X-ray diffraction (XRD), and X-ray photoelectron spectroscopy (XPS). Fig. S1† shows the HRTEM images of Au NBPs. The spacing between the lattice fringes as calculated from HRTEM images was found to be 0.234 nm which is ascribed to the 111 facets of bipyramids.[51] The EDX pattern of Au NBPs (Fig. S2†) reveals that mostly Au is present in Au NBPs with a very little trace of Ag (0.67%). Furthermore, the XRD patterns as depicted in Fig. S3(a)† reveal four prominent peaks of (111), (200), (220), and (311) corresponding to the cubic structure of Au.[52] The XPS analysis of Au NBPs (Fig. S3(b)†) shows double Au 4f peaks where the peak at 84 eV reveals the onset of Au^+ ions as described in a previous report.[53]

After the successful synthesis of Au NBPs, they were functionalized with thiolated oligonucleotides (Table S1†) with modifications to a method reported previously.[47] The procedure of DNA functionalization of Au NBPs is schematically illustrated in Fig. S4(a).† The deprotected thiolated DNA sequences 5′-SH-CGTCGTATTCGATAGCTTAG-3′ and 5′-SH-TTGGTGGTGGTGGTGGTGGT-3′ were incubated with Au NBPs in 5 × TBE buffer overnight followed by slow salt (5 M NaCl) addition

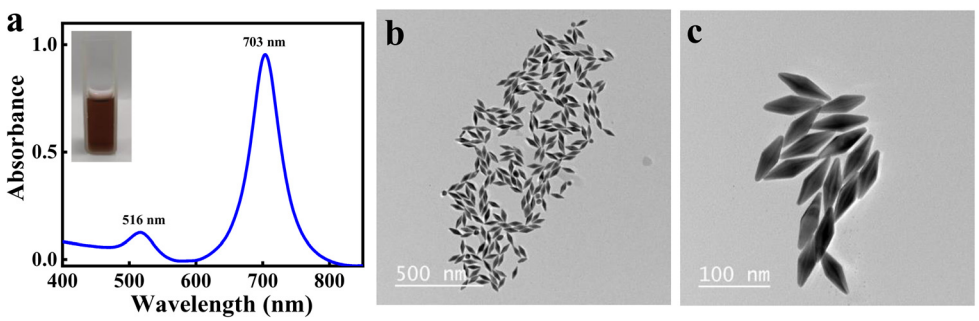

Fig. 1 (a) UV-Vis spectrum of Au NBPs, and (b) and (c) TEM images of Au NBPs.

until a final concentration of 400 mM is reached. The UV-Vis spectra of DNA functionalized Au NBPs depicted a red shift of ~9 nm (Fig. S4(b)†). The as prepared DNA functionalized Au NBPs were stable in NaCl with a high salt concentration of 500 mM, required for immobilization on DNA origami (Fig. S4(c)†).

3.2 Design of the Au NBP monomer and dimer structures on DNA origami

The assembly of Au NBPs on DNA origami is illustrated in Scheme 1. Au NBPs were self-assembled in monomer and dimer configurations on DNA origami using dangling capturing ssDNA extensions protruding from DNA origami having a complementary sequence with ssDNA modified Au NBPs. Two different sets of capturing strand sequences on each origami monomer were used to assemble Au NBPs in the dimer configuration while the capturing strands on only one origami monomer were used to prepare the Au NBP monomer. The conjugation sites on each origami monomer consist of a set of seven staple strands extended at the 3′ end having a sequence complementary to the thiolated DNA sequence coated on Au NBPs. Thus, a precise site-specific customized arrangement of Au NBPs on DNA origami was acquired as a result of the hybridization interactions between the complementary strands. The positions of capturing strands are illustrated in Fig. S5† with detailed sequences in Table S2.† The rectangular DNA origami monomer (90 nm × 60 nm) and dimer (180 nm × 60 nm) were prepared according to our previous report.[25] The AFM images as depicted in Fig. S6† confirmed the formation of a DNA origami monomer and dimer. Fig. 2(a) and (b) show the AFM images of the Au NBP monomer and dimer on DNA origami indicating the successful immobilization of Au NBPs on DNA origami. The TEM imaging (Fig. 2(c) and (d)) further confirmed the assembly of Au NBPs on DNA origami in monomer and dimer configurations. The rectangular DNA origami template is clearly visible in the case of the Au NBP monomer while it got hidden in the Au NBP dimer. The average gap between the Au NBP dimer as calculated from different TEM images was 4.8 ± 1 nm. The additional TEM images of the Au NBP monomer and dimer on DNA origami are included in Fig. S7 and S8,† respectively. The yields of the Au NBP monomer and dimer assemblies as calculated from different TEM images were 65% and 62%, respectively.

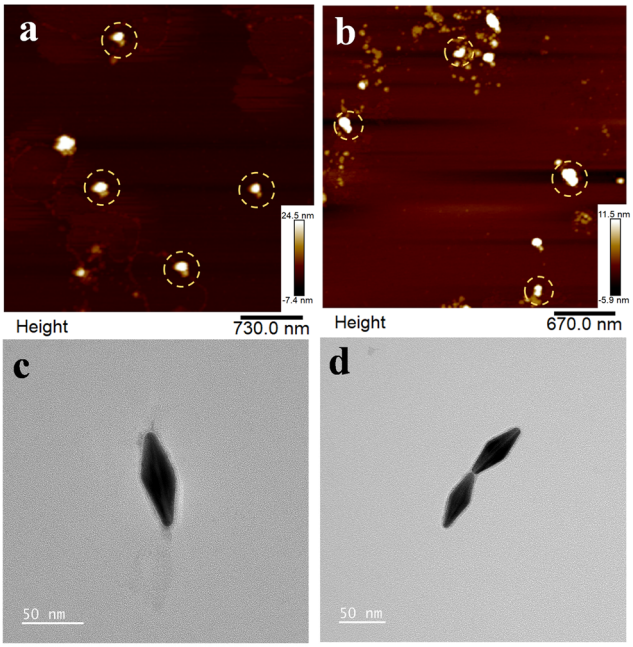

Fig. 2 AFM images of Au NBPs: (a) monomer and (b) dimer, and TEM images of Au NBPs: (c) monomer and (d) dimer.

3.3 SERS enhancement of ThT using Au NBP nanoantennas on DNA origami

The assemblies of Au NBPs on DNA origami are expected to generate strong plasmonic enhancement and thus the potential of Au NBP nanoantennas was explored as a sensing platform by SERS enhancement of ThT, a well-known marker for amyloid fibril formation. The design of the SERS platform (Scheme 2) was based on the specific detection of ThT using a G-rich DNA sequence at the center of DNA origami. ThT is known to specifically interact with G-rich DNA sequences, prompting the formation of G-rich DNA to the G-quadruplex complex and subsequently binding to the complex.[14,54] The design strategy for SERS includes the replacement of one staple in the middle of DNA origami with a G-rich DNA sequence. When ThT is added, it recognizes the G-rich DNA sequence inducing the formation of a G-Quadruplex followed by the intercalation of ThT into a G-Quadruplex complex. The 29-mer DNA sequence 5′-AGTCCGTGGTAGGGCAGGTTGGGGTGACT-3′ was used for the SERS based detection of ThT.[55]

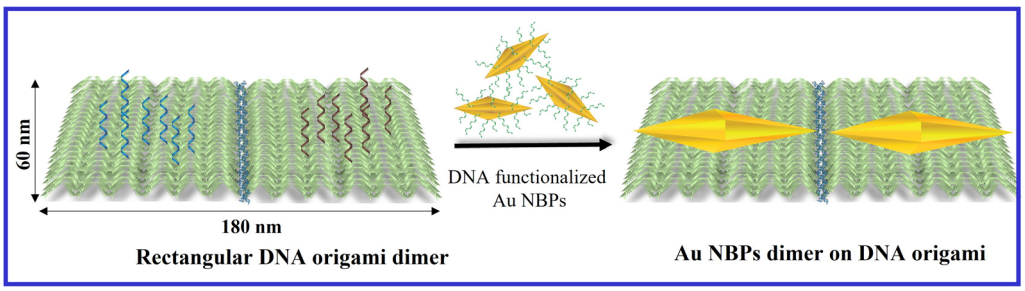

Scheme 1 Schematic depiction of the immobilization of Au NBPs on dimerized DNA origami.

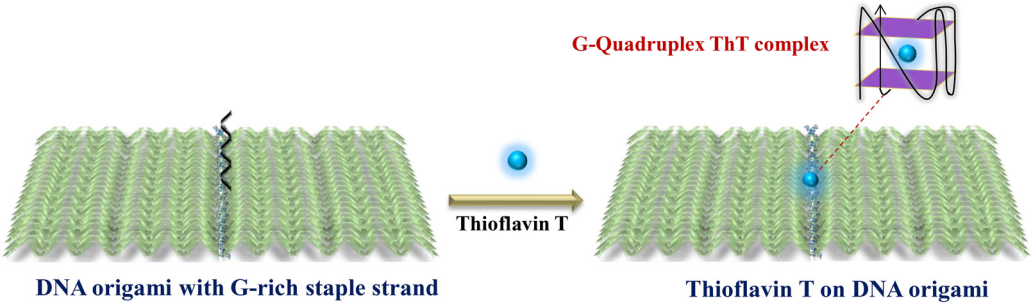

Scheme 2 Schematic illustration of the immobilization of the ThT dye on DNA origami.

After the formation of the ThT-G Quadruplex complex on DNA origami, we conducted single molecule confocal measurements as a quantitative tool to determine the attachment of ThT dye molecules on DNA origami. Single molecule fluorescence spectroscopy is a powerful imaging technique that can localize and track single fluorophores allowing the study of in-depth insights into a system at the molecular level.[56–58] Thus, we explored the single molecule confocal fluorescence microscopy to estimate the stoichiometry of ThT dye molecules on DNA origami. The sample for confocal measurements was prepared using Lab-Tek chambered coverglass *via* specific biotin–NeutrAvidin interactions (staple positions in Table S3†). The ThT dye is a rotor molecule that consists of a pair of benzothiazole (BT) and dimethylaminobenzene (DMB) rotating freely around the C–C bond (Fig. S9†).[6] However, when it is intercalated in the G-Quadruplex complex, the dye adapts a rigid and planar form which restricts its rotation, thereby increasing the fluorescence.[14] The UV-Vis absorption spectrum of ThT is depicted in Fig. S10.† The representative fluorescence intensity, fluorescence lifetime imaging microscopy (FLIM) images, and their corresponding fluorescence transients using a 405 nm excitation laser source are depicted in Fig. 3. The individual bright spots depicted in the images (Fig. 3(a) and (b)) represent the molecules of the ThT dye. When a dye molecule is subjected to prolonged illumination, loss of fluorescence is observed resulting in a sudden drop of the fluorescence intensity to the background level, known as photobleaching.[59,60] Thus, by monitoring the photobleaching steps in the fluorescence transients, the number of molecules can be predicted. We observed the photobleaching of the ThT dye in the intensity time-traces (Fig. 3(c)) to estimate the stoichiometry of ThT dye molecules on DNA origami. As observed from the intensity time-trace profiles, single-step photobleaching was observed which predicted the presence of a single ThT dye molecule within the nanoantenna assembly. Different representative time traces are shown in Fig. S11† which depicts the photobleaching of the dye molecules in one step. Fig. S12 and S13† depict the FLIM images and corresponding time trace profiles of the Au NBP monomer and dimer assemblies with initial ThT concentrations of 40 nM and 20 nM, respectively. The time trace profiles of several molecules were analyzed to estimate the number of ThT dye molecules in Au

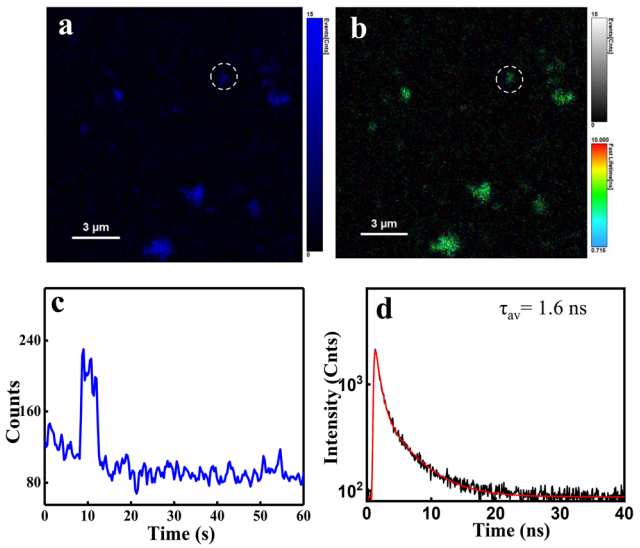

Fig. 3 (a) Fluorescence intensity, (b) fluorescence lifetime (FLIM) images, and the corresponding (c) time trace, and (d) decay profile of the ThT dye using the Au NBP monomer on DNA origami.

NBP nanoantennas. In addition to single step photobleaching, the time trace profile also showed photobleaching in two steps (Fig. S12(e) and S13(f)†), and multiple steps (Fig. S12(l)†) indicating the presence of two molecules as well as a few aggregated structures in some assemblies. The yield of the calculated number of molecules is depicted in Table S5.† It was found from time traces that the single molecules were having a yield of 86% with a 9% fraction of two molecules and 5% multiple molecules. This indicates that mostly single molecules of the ThT dye are immobilized on DNA origami indicating a 1 : 1 stoichiometry of the ThT-G Quadruplex complex.

There have been previous reports where 1 : 1 and 1 : 2 G-Quadruplex ThT modes are described,[14,61,62] however in the present study, single molecule fluorescence analysis showed the presence of a majority of the 1 : 1 G-Quadruplex/ThT complex. The decay profile showed an average lifetime of 1.6 ns for the ThT dye on DNA origami.

The SERS measurements of ThT using Au NBP nanoantennas were conducted on Si wafer using a 633 nm laser excitation

source at 0.5 mW laser power with 1 second accumulation time. The reference spectrum of ThT was recorded using the same parameters using ThT adsorbed on the surface of 80 nm spherical Ag NPs as depicted in Fig. 4(a). The characteristic peaks at 700, 742, 794, 1033, 1129, 1400, 1536, and 1600 cm^{-1} obtained in the reference spectrum correlated well with the peaks of ThT in previous reports.[6,22–24] The bands at 700 and 742 cm^{-1} are assigned to the CCC (ring I) bending and CCC bending, respectively. The peaks at 794 and 1129 cm^{-1} are assigned to CH_3 (ring II) bending.[22] The peaks at 1033 and 1402 cm^{-1} are assigned to CCC bending and methyl bending (ring I, II and III), respectively, and those at 1536 and 1600 cm^{-1} are assigned to CC (ring III) vibrations, respectively. The assignment of the corresponding peaks is given in Table S4.† The SERS spectra of ThT using the Au NBP monomer and dimer on DNA origami are depicted in Fig. 4(b) and (c). The peak corresponding to CC vibrations shifted from 1600 to 1620 cm^{-1} in the case of Au NBP nanoantennas along with a shift in the peak from 1400 to 1384 cm^{-1} and from 1129 to 1177 cm^{-1}. The peaks at 1476 cm^{-1} and 1477 cm^{-1} can be ascribed to the formation of a G-Quadruplex, indicative of C8═N7–H2 deformation (band of Guanine).[63] Additional SERS spectra of ThT using an Au NBP dimer on DNA origami are illustrated in Fig. S14.† The peak positions in the SERS spectra of ThT in the presence of Au NBP monomer and dimer structures were found to be similar; however, they differ from the SERS spectrum of Ag NPs. This can be because of interactions of ThT with the G-Quadruplex complex in the case of nanoantennas, while for the reference SERS spectrum, the ThT dye molecule is in the vicinity of bare Ag NPs. When ThT is in proximity to Ag NPs, the S atom of the BT moiety interacts with the metal surface.[6] However, when ThT is intercalated in the G-Quadruplex configuration, its internal rotation is blocked, providing no direct interactions with the metal surface. Thus, the shifting of the peaks indicates the intercalation of the ThT dye molecule in the G-Quadruplex complex.

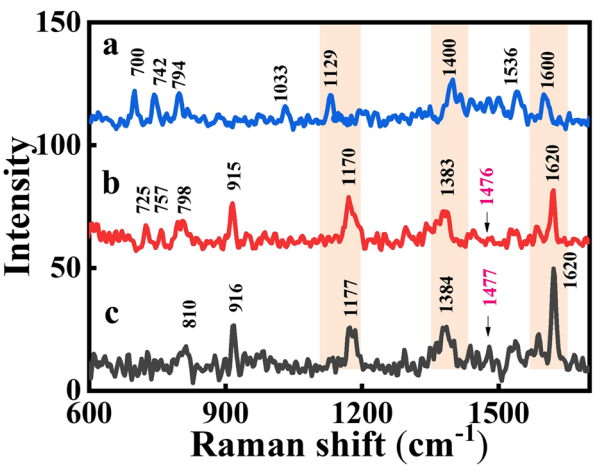

Fig. 4 SERS measurements of ThT using (a) 80 nm spherical Ag NPs, (b) Au NBP monomer, and (c) Au NBP dimer on DNA origami.

In the present study, first, AFM imaging was done to identify the assembled Au NBP nanoassemblies followed by SERS measurements of the ThT dye using Au NBP nanoantenna structures. In order to estimate the number of molecules contributing to the SERS signal of ThT, we monitored the number of nanoantenna assemblies present in the laser confocal area, which is 1 μm^2.[25] It can be seen from the AFM images (Fig. 2(a) and (b)) that only one nanoantenna assembly is estimated in an area of 1 μm^2. Thus, only one nanoantenna assembly is present in the laser confocal area. An AFM correlated Raman image is further shown in Fig. S15.† Since a single ThT dye is present in one nanoantenna assembly, which is also confirmed by single step photobleaching in single molecule fluorescence transient measurements (Fig. 3(c)), we can confirm that SERS signature peaks are originating from only one ThT dye molecule. Hence, it can be concluded that the enhancement in the SERS signal of the ThT dye is due to the specific immobilization of a single dye molecule in the plasmonic hotspot of Au NBP nanoantennas assembled on DNA origami.

Furthermore, concentration dependent SERS and single molecule fluorescence confocal measurements of the ThT dye were also performed using Au NBP monomer assemblies to estimate the limit of detection (LOD). The concentration dependent measurements revealed that the signal of the ThT dye was obtained until a concentration of 0.1 nM. Concentration dependent SERS and single molecule fluorescence confocal measurements are presented in Fig. S16.†

To further examine the plasmonic effect of nanoantennas in the signal enhancement of ThT, Raman measurements were performed using ThT on DNA origami in the absence of Au NBPs. As shown in Fig. S17,† no characteristic peaks of ThT were observed without NBPs demonstrating the major role of nanostructures in signal enhancement. We further demonstrated the role of a G-Quadruplex in the specific detection of ThT and prepared a sample replacing the G-rich strand at the center of DNA origami with two different branching strand sequences without a G-rich sequence in the AuBPs–DNA origami assembly. In this case, no prominent SERS signatures of ThT were obtained, which depicted the crucial role of intercalation of ThT in the G-Quadruplex complex for the enhancement of the SERS signal (Fig. S18†). Furthermore, control measurements done using different concentrations of the dye showed no significant peaks as depicted in Fig. S19.†

While there have been developments of various G-Quadruplex based fluorescence assays where ThT exhibited enhanced fluorescence upon intercalation into the G-Quadruplex complex,[14,55] not much interest is devoted to the SERS based detection of ThT using a G-Quadruplex based sensing strategy. SERS based detection offers the advantage of investigating specific analytes from complex mixtures, serving as highly sensitive diagnostic platforms for biomolecule detection.[17] Previously, the vibrational characteristics of ThT on the surface of Ag nanoparticles using SERS were demonstrated by Lopez-Tobar *et al.*[6] Furthermore, Maiti *et al.* demonstrated the SERS based detection of ThT using Au NPs, Ag NPs and Ag

Table 1 Comparison of different methods for ThT detection

Material	Method	Limit of detection (LOD)	Ref.
Au NPs, Ag NPs, and Ag coated films	SERS	0.1 nM	22
Polymeric films having multi-branched NPs	SERS	0.5 pg ml^{-1}	23
Hollow Au/Ag nanostars	SERS	10 nM	24
Ag NPs	SERS	1 nM	4
Au NBP nanoantennas	SERS	0.1 nM	Present paper

coated films with 100 pM sensitivity.[22] Also, hollow Au/Ag nanostars[24] and multibranched nanopillar surfaces[23] have been used in the past for the detection of ThT. The comparison of the limits of detection of the ThT dye using different materials is presented in Table 1. The previous reports demonstrate the design of the SERS substrate based on the adsorption of ThT. Herein, specific detection of single ThT is demonstrated using a high-performance biocompatible SERS substrate precisely engineered using the DNA origami technique. The as-designed low-cost, reproducible, and highly efficient SERS substrate show potential for the highly sensitive detection of important biomolecules offering unprecedented opportunities in the development of various point-of-care clinical applications.

4 Conclusions

In summary, we demonstrate the design of self-assembled Au NBP monomer and dimer plasmonic nanoantennas assembled using DNA origami. The plasmonic coupled AuNBPs with sharp tips give rise to extremely strong electromagnetic enhancement, demonstrated by the ultrasensitive and specific detection of ThT, a marker for amyloid fibril formation. The quantification of the ThT dye molecule as estimated by single molecule confocal measurements suggested the presence of single ThT molecules incorporated into DNA origami. The designed nanoantennas were able to detect the spectroscopic SERS signatures of ThT, specifically positioned at the plasmonic hotspot of Au NBPs using a G-Qudruplex based strategy. Such DNA origami assembled plasmonic nanoantennas possess the profound capability for a strongly enhanced plasmonic response serving as a versatile platform in the context of biomolecular detection for disease diagnosis.

Author contributions

T. S. devised and supervised the project. T. S., C. K. and V. K. devised the experiments, analyzed the data, and wrote the manuscript. C. K. and S. R. performed the experiments. M. S. contributed towards the measurements of samples. All the authors discussed the results and contributed to the preparation of the manuscript.

Conflicts of interest

The authors declare no conflict of interest.

Acknowledgements

T. S. is thankful to the Department of Science and Technology (SERB Project-CRG/2019/005481) for financial support and the INST for the infrastructural facility. C. K. is thankful to the INST for a senior research fellowship. V. K. is thankful to the CSIR for a senior research fellowship and the CNSNT (Panjab University) for PhD registration. S. R. and M. S. acknowledge the INST for a junior research fellowship.

References

1 T. P. J. Knowles, M. Vendruscolo and C. M. Dobson, *Nat. Rev. Mol. Cell Biol.*, 2014, **15**, 384–396.
2 O. Hansson, *Nat. Med.*, 2021, **27**, 954–963.
3 R. N. Rambaran and L. C. Serpell, *Prion*, 2008, **2**, 112–117.
4 E. H. Koo, P. T. Lansbury and J. W. Kelly, *Proc. Natl. Acad. Sci. U. S. A.*, 1999, **96**, 9989–9990.
5 T. Sinnige, *Chem. Sci.*, 2022, **13**, 7080–7097.
6 E. Lopez-Tobar, M. Antalik, D. Jancura, M. V. Cañamares, A. García-Leis, D. Fedunova, G. Fabriciova and S. Sanchez-Cortes, *J. Phys. Chem. C*, 2013, **117**, 3996–4005.
7 V. I. Stsiapura, A. A. Maskevich, V. A. Kuzmitsky, V. N. Uversky, I. M. Kuznetsova and K. K. Turoverov, *J. Phys. Chem. B*, 2008, **112**, 15893–15902.
8 C. Rodríguez-Rodríguez, A. Rimola, L. Rodríguez-Santiago, P. Ugliengo, Á. Álvarez-Larena, H. Gutiérrez-de-Terán, M. Sodupe and P. González-Duarte, *Chem. Commun.*, 2010, **46**, 1156–1158.
9 N. Amdursky, Y. Erez and D. Huppert, *Acc. Chem. Res.*, 2012, **45**, 1548–1557.
10 C. Xue, T. Y. Lin, D. Chang and Z. Guo, *R. Soc. Open Sci.*, 2017, **4**, 160696.
11 L. Qin, J. Vastl and J. Gao, *Mol. Biosyst.*, 2010, **6**, 1791–1795.
12 F. Gorka, S. Daly, C. M. Pearson, E. Bulovaite, Y. P. Zhang, A. Handa, S. G. N. Grant, T. N. Snaddon, L.-M. Needham and S. F. Lee, *J. Phys. Chem. B*, 2021, **125**, 13710–13717.
13 X. Liu, X. Hua, Q. Fan, J. Chao, S. Su, Y.-Q. Huang, L. Wang and W. Huang, *ACS Appl. Mater. Interfaces*, 2015, **7**, 16458–16465.
14 J. Mohanty, N. Barooah, V. Dhamodharan, S. Harikrishna, P. I. Pradeepkumar and A. C. Bhasikuttan, *J. Am. Chem. Soc.*, 2013, **135**, 367–376.
15 N. P. W. Pieczonka and R. F. Aroca, *Chem. Soc. Rev.*, 2008, **37**, 946–954.
16 S. Schlücker, *Angew. Chem., Int. Ed.*, 2014, **53**, 4756–4795.

17 K. C. Bantz, A. F. Meyer, N. J. Wittenberg, H. Im, Ö. Kurtuluş, S. H. Lee, N. C. Lindquist, S.-H. Oh and C. L. Haynes, *Phys. Chem. Chem. Phys.*, 2011, **13**, 11551–11567.
18 R. A. Tripp, R. A. Dluhy and Y. Zhao, *Nano Today*, 2008, **3**, 31–37.
19 T. J. Moore, A. S. Moody, T. D. Payne, G. M. Sarabia, A. R. Daniel and B. Sharma, *Biosensors*, 2018, **8**, 46.
20 W. Yang, K. J. Si, P. Guo, D. Dong, D. Sikdar, M. Premaratne and W. Cheng, *J. Anal. Test.*, 2017, **1**, 335–343.
21 M. Yilmaz, E. Senlik, E. Biskin, M. S. Yavuz, U. Tamer and G. Demirel, *Phys. Chem. Chem. Phys.*, 2014, **16**, 5563–5570.
22 N. Maiti, R. Chadha, A. Das and S. Kapoor, *Spectrochim. Acta, Part A*, 2015, **149**, 949–956.
23 S. Altuntas and F. Buyukserin, *J. Raman Spectrosc.*, 2018, **49**, 1247–1256.
24 A. Garcia-Leis, A. Torreggiani, J. V. Garcia-Ramos and S. Sanchez-Cortes, *Nanoscale*, 2015, **7**, 13629–13637.
25 S. Tanwar, K. K. Haldar and T. Sen, *J. Am. Chem. Soc.*, 2017, **139**, 17639–17648.
26 J. Prinz, C. Heck, L. Ellerik, V. Merk and I. Bald, *Nanoscale*, 2016, **8**, 5612–5620.
27 T. Tørring, N. V. Voigt, J. Nangreave, H. Yan and K. V. Gothelf, *Chem. Soc. Rev.*, 2011, **40**, 5636–5646.
28 Q. Jiang, S. Liu, J. Liu, Z.-G. Wang and B. Ding, *Adv. Mater.*, 2019, **31**, 1804785.
29 G. Kong, M. Xiong, L. Liu, L. Hu, H.-M. Meng, G. Ke, X.-B. Zhang and W. Tan, *Chem. Soc. Rev.*, 2021, **50**, 1846–1873.
30 M. Dass, F. N. Gür, K. Kołątaj, M. J. Urban and T. Liedl, *J. Phys. Chem. C*, 2021, **125**, 5969–5981.
31 V. Kaur, S. Tanwar, G. Kaur and T. Sen, *ChemPhysChem*, 2021, **22**, 160–167.
32 V. Kaur, M. Sharma and T. Sen, *Front. Chem.*, 2021, **9**, 1–11.
33 S. Tanwar, V. Kaur, G. Kaur and T. Sen, *J. Phys. Chem. Lett.*, 2021, **12**, 8141–8150.
34 S. Lee, P. Kumar, Y. Hu, G. J. Cheng and J. Irudayaraj, *Chem. Commun.*, 2015, **51**, 15494–15497.
35 T. H. Chow, N. Li, X. Bai, X. Zhuo, L. Shao and J. Wang, *Acc. Chem. Res.*, 2019, **52**, 2136–2146.
36 X. Zhu, H. K. Yip, X. Zhuo, R. Jiang, J. Chen, X.-M. Zhu, Z. Yang and J. Wang, *J. Am. Chem. Soc.*, 2017, **139**, 13837–13846.
37 R. Pardehkhorram, S. Bonaccorsi, H. Zhu, V. R. Gonçales, Y. Wu, J. Liu, N. A. Lee, R. D. Tilley and J. J. Gooding, *Chem. Commun.*, 2019, **55**, 7707–7710.
38 M. U. Amin, L. Li, R. Zhang and J. Fang, *Talanta*, 2023, **251**, 123800.
39 J. Dong, Y. Zhou, J. Pan, C. Zhou and Q. Wang, *Chem. Commun.*, 2021, **57**, 6201–6204.
40 Y. Liu, Z. Li, Z. Yin, H. Zhang, Y. Gao, G. Huo, A. Wu and L. Zeng, *ACS Appl. Mater. Interfaces*, 2020, **12**, 14866–14875.
41 T. Fu, C. Du, Y. Chen, R. Zhang, Y. Zhu, L. Sun and D. Shi, *Plasmonics*, 2021, **16**, 485–491.
42 X. Yang, Y. Liu, S. H. Lam, J. Wang, S. Wen, C. Yam, L. Shao and J. Wang, *Nano Lett.*, 2021, **21**, 8205–8212.
43 M. U. Amin, R. Zhang, L. Li, H. You and J. Fang, *Anal. Chem.*, 2021, **93**, 7657–7664.
44 R. Deska, P. Obstarczyk, K. Matczyszyn and J. Olesiak-Bańska, *J. Phys. Chem. Lett.*, 2021, **12**, 5208–5213.
45 A. Sánchez-Iglesias, N. Winckelmans, T. Altantzis, S. Bals, M. Grzelczak and L. M. Liz-Marzán, *J. Am. Chem. Soc.*, 2017, **139**, 107–110.
46 Q. Li, X. Zhuo, S. Li, Q. Ruan, Q. H. Xu and J. Wang, *Adv. Opt. Mater.*, 2015, **3**, 801–812.
47 C. Shen, X. Lan, X. Lu, T. A. Meyer, W. Ni, Y. Ke and Q. Wang, *J. Am. Chem. Soc.*, 2016, **138**, 1764–1767.
48 M. Liu and P. Guyot-Sionnest, *J. Phys. Chem. B*, 2005, **109**, 22192–22200.
49 Q. Li, X. Zhuo, S. Li, Q. Ruan, Q.-H. Xu and J. Wang, *Adv. Opt. Mater.*, 2015, **3**, 801–812.
50 Q. Li, R. Jiang, T. Ming, C. Fang and J. Wang, *Nanoscale*, 2012, **4**, 7070–7077.
51 J.-H. Lee, K. J. Gibson, G. Chen and Y. Weizmann, *Nat. Commun.*, 2015, **6**, 7571.
52 C. Fang, G. Zhao, Y. Xiao, J. Zhao, Z. Zhang and B. Geng, *Sci. Rep.*, 2016, **6**, 36706.
53 P. Chen, G. Wang, C. Hao, W. Ma, L. Xu, H. Kuang, C. Xu and M. Sun, *Chem. Sci.*, 2022, **13**, 10281–10290.
54 A. C. Bhasikuttan and J. Mohanty, *Chem. Commun.*, 2015, **51**, 7581–7597.
55 X. Liu, X. Hua, Q. Fan, J. Chao, S. Su, Y.-Q. Huang, L. Wang and W. Huang, *ACS Appl. Mater. Interfaces*, 2015, **7**, 16458–16465.
56 S. Shashkova and M. C. Leake, *Biosci. Rep.*, 2017, **37**, 1–19.
57 E. J. Peterman, H. Sosa and W. E. Moerner, *Annu. Rev. Phys. Chem.*, 2004, **55**, 79–96.
58 P. Tinnefeld and M. Sauer, *Angew. Chem., Int. Ed.*, 2005, **44**, 2642–2671.
59 E. M. S. Stennett, M. A. Ciuba and M. Levitus, *Chem. Soc. Rev.*, 2014, **43**, 1057–1075.
60 K. Tsekouras, T. C. Custer, H. Jashnsaz, N. G. Walter and S. Pressé, *Mol. Biol. Cell*, 2016, **27**, 3601–3615.
61 H. Cai, C. Zhou, Q. Yang, T. Ai, Y. Huang, Y. Lv, J. Geng and D. Xiao, *Chin. Chem. Lett.*, 2018, **29**, 531–534.
62 S. Verma, S. A. Ghuge, V. Ravichandiran and N. Ranjan, *Spectrochim. Acta, Part A*, 2019, **212**, 388–395.
63 A. Dutta, K. Tapio, A. Suma, A. Mostafa, Y. Kanehira, V. Carnevale, G. Bussi and I. Bald, *Nanoscale*, 2022, 16467–16478.